# Computational Predictions of Binding Affinities to Dihydrofolate Reductase: Synthesis and Biological Evaluation of Methotrexate Analogues

Malin Graffner-Nordberg,[†] John Marelius,[‡] Sofie Ohlsson,[§] Åsa Persson,[§] Göte Swedberg,[#] Paul Andersson,[§] Sven E. Andersson,[⊥] Johan Åqvist,[‡] and Anders Hallberg*[,†]

*Department of Organic Pharmaceutical Chemistry, Uppsala Biomedical Center, Uppsala University, Box 574, SE-751 23 Uppsala, Sweden; Department of Cell and Molecular Biology, Uppsala Biomedical Center, Uppsala University, Box 596, SE-751 24 Uppsala, Sweden; Discovery, AstraZeneca R&D Lund, SE-221 87 Lund, Sweden; Department of Pharmaceutical Microbiology, Uppsala Biomedical Center, Uppsala University, Box 581, SE-751 23 Uppsala, Sweden; and Department of Internal Medicine, Lund University Hospital, SE-221 86 Lund, Sweden*

*Received April 3, 2000*

The relative binding affinities to human dihydrofolate reductase of four new potential antifolates, containing ester linkages between the two aromatic systems, were estimated by free energy perturbation simulations. The ester analogue, predicted to exhibit the highest binding affinity to human dihydrofolate reductase, and a reference ester (more structurally related to methotrexate) were synthesized. As deduced from the measured $IC_{50}$ values, the calculated ranking of the ligands was correct although a greater difference in affinity was indicated by the experimental measurements. Among the new antifolates the most potent inhibitor exhibited a similar pharmacokinetic profile to methotrexate but lacked activity in a complex antiarthritic model in rat in vivo.

## Introduction

Dihydrofolate reductase (DHFR) is a well-established target for drug intervention. Several inhibitors are approved as therapeutic agents against a variety of pathological disorders. Thus, the classical antifolate, methotrexate (MTX), is used in cancer therapy and frequently for the treatment of rheumatoid arthritis[1−3] and psoriasis.[4−6] MTX is also reported to be effective against steroid-resistant asthma[7,8] and inflammatory bowel diseases.[9,10] Research programs aimed at identifying new classical antifolates have been pursued, and numerous new derivatives with potential use against, for example, rheumatoid arthritis have been reported.[11] The nonclassical lipophilic inhibitors have been used for a long time against bacterial infections (e.g., trimethoprim) and in the treatment of malaria (e.g., pyrimethamine). Considerable efforts are at present devoted to identifying selective DHFR inhibitors for treatment of infections caused by *Pneumocystis carinii* and *Toxoplasma gondii*, two major opportunistic pathogens often found in patients with acute AIDS and other immunodeficiency disorders.[12] Trimetrexate[13] and piritrexim[14] are two potent, lipophilic, nonclassical inhibitors from the new generation of antifolates used in the clinic. In a previous metabolism study, a series of model compounds was investigated with the objective of defining the molecular structural factors which affect the rate of enzymatic ester cleavage and the tissue selectivity of hydrolytic metabolism.[15] The model compounds examined comprised bicyclic aromatic units connected by an ester-containing bridge to a second aromatic ring. It was revealed that compounds containing 2,4-diaminoquinazoline as the bicyclic element only sluggishly undergo enzymatic hydrolyses in human and rat liver S9 fractions as well as in human duodenal mucosa homogenate and, in particular, in human blood leukocytes, the latter being target cells for immunosuppressive drugs. These findings encouraged us to synthesize and evaluate an analogue to MTX, where the methyleneamino bridge was substituted with a suitable ester unit, as a potential metabolically stable inhibitor of human DHFR possessing a new linker type.

We herein report the calculations of relative binding affinities from free energy perturbation simulations that guided the selection of the target compound to be synthesized, the subsequent synthesis, and the biological evaluation in a human DHFR assay. Furthermore, to assess the metabolic stability of the ester bond of the selected compound, a pharmacokinetic study was performed and the compound was thereafter evaluated in an antigen-induced arthritis (AIA) model.

## Results

**Computational Prediction of Binding Affinities.** Organic synthesis is time-consuming, and methods allowing reliable predictions of affinity and specificity of ligands prior to synthesis would be of paramount value in the drug discovery process. Even with a three-dimensional structure of the target available, computational predictions of binding affinity of a new ligand are difficult when the exact structure of the ligand−enzyme complex is unknown. A range of different methods to approach this problem has been developed,[16] including methods for scoring putative inhibitors from single conformations of ligand−enzyme complexes[17] and estimations of absolute binding free energies using

* To whom correspondence should be addressed. Tel: +46 18 4714284. Fax: +46 18 4714976. E-mail: Anders.Hallberg@bmc.uu.se.
[†] Department of Organic Pharmaceutical Chemistry, Uppsala University.
[‡] Department of Cell and Molecular Biology, Uppsala University.
[§] AstraZeneca R&D Lund.
[#] Department of Pharmaceutical Microbiology, Uppsala University.
[⊥] Lund University Hospital.

10.1021/jm0009639 CCC: $19.00 
Published on Web 10/04/2000

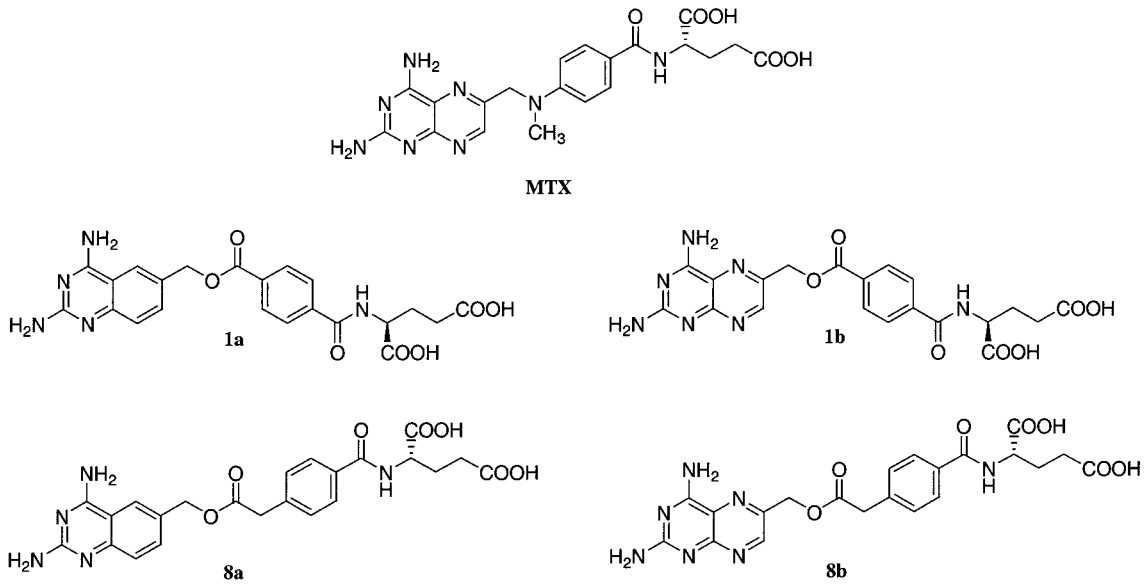


**Figure 1.** MTX and four potential inhibitors of DHFR used in the calculations of binding free energies.

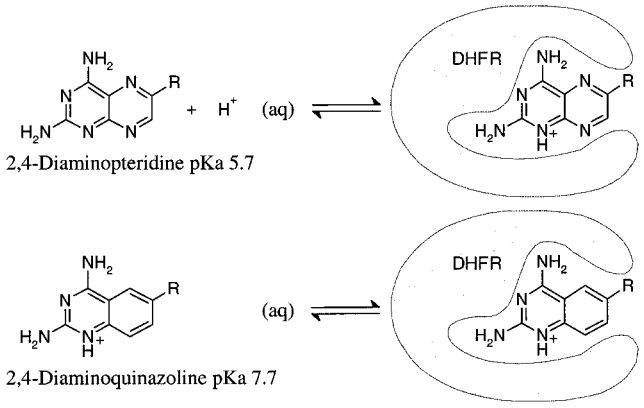


**Figure 2.** Binding processes of 2,4-diaminopteridines and 2,4-diaminoquinazolines. The former is not protonated at N1 in water at neutral pH, and protonation upon binding is associated with a free energy cost.

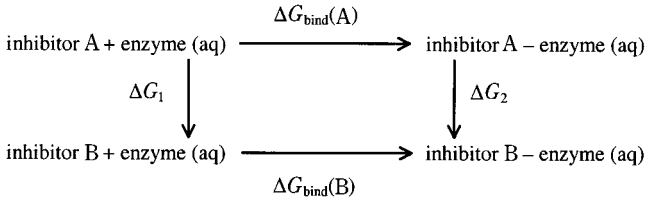


**Figure 3.** Thermodynamic cycle for relative binding affinity.

linear interaction energy methods based on conformational sampling by molecular dynamics (MD) simulations.[18]

We used relative binding affinities calculated from free energy perturbation (FEP) simulations[19] for the selection of one of the four esters depicted in Figure 1 as the compound likely to inhibit human DHFR most efficiently. Binding free energies of the esters **1a,b** relative to the reference compound MTX as well as of **8a**,**b** relative to **1a**,**b** were calculated. In this way the largest perturbations (MTX → **8a**,**b**) are divided into two steps with the two compounds **1a**,**b** as intermediates along the FEP paths. Compound **1b**, which is structurally most similar to MTX, and the 2,4-diaminoquinazoline **1a** both contain the same bridge (methyleneoxycarbonyl) as in the compounds previously examined in the metabolism study.[15] The other two candidates for synthesis, the quinazoline **8a** and the pteridine derivative **8b**, possessed four-atom bridges (Figure 1). Energy is required to protonate the pteridines upon binding, whereas the quinazolines are protonated also in solution at neutral pH, as illustrated in Figure 2.

MD simulations, during which MTX was gradually transformed into **1a** or **1b** and **1a**,**b** into **8a**,**b**, respectively, were performed. From a pair of simulations, one of the inhibitors free in water and the other comprising the inhibitor bound to the solvated enzyme, the relative free energy of binding can be calculated using the thermodynamic cycle shown in Figure 3. The p$K_a$ values of the bicyclic element of the 2,4-diaminopteridines and the 2,4-diaminoquinazolines, respectively, differ by about 2 units.[20] Energy is required to protonate the pteridines upon binding, whereas the quinazolines are protonated in solution at pH 6.9 (used in $IC_{50}$ determinations), as illustrated in Figure 2. To compare the energetics of the bound and free states of the ligand using the thermodynamic cycle, the same protonation state must be used in both environments. All simulations were thus carried out using the protonation state of the bound ligands, and the free energy for protonation in water was added as a correction. The resulting free energies, which are averages over independent simulations of the forward and reverse transformation simulations, are summarized in Table 1. The simulations identified the quinazoline ester **1a** as about 4 times more potent as an inhibitor of human DHFR than the pteridine ester **1b** but less potent than MTX by 1 order of magnitude (see Table 2). A methylene extension was found to reduce the enzyme affinity as deduced from calculations. Thus, the quinazoline compound **8a** was predicted to be approximately equipotent to **1b,** while the pteridine **8b** was predicted to have the lowest affinity among the compounds studied. We finally selected **1a** as the first candidate for synthesis and biological evaluation. Furthermore, the lower affinity of **1b** that was predicted by the FEP calculations was not obvious from modeling, and we therefore felt prompted to also synthesize **1b** as a reference compound

**Scheme 1**[a]

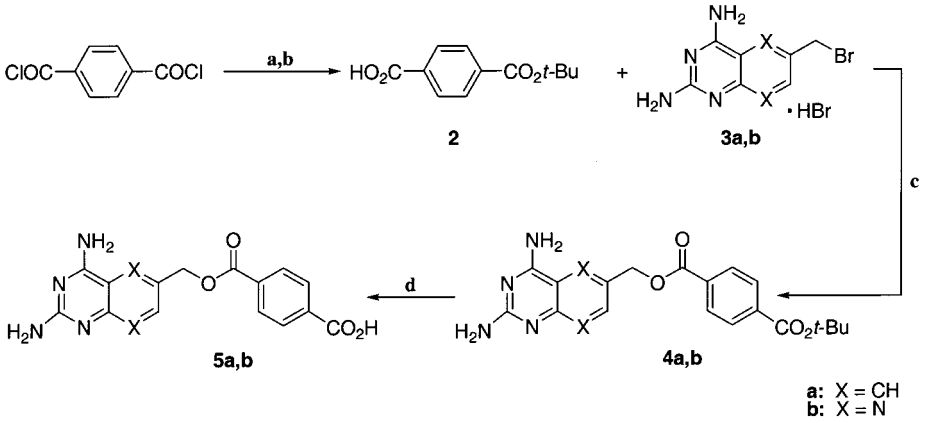


[a] Reagents and conditions: (a) *tert*-butyl alcohol, pyridine; (b) KOH, *tert*-butyl alcohol; (c) cesium carbonate, DMF; (d) TFA.

**Scheme 2**[a]

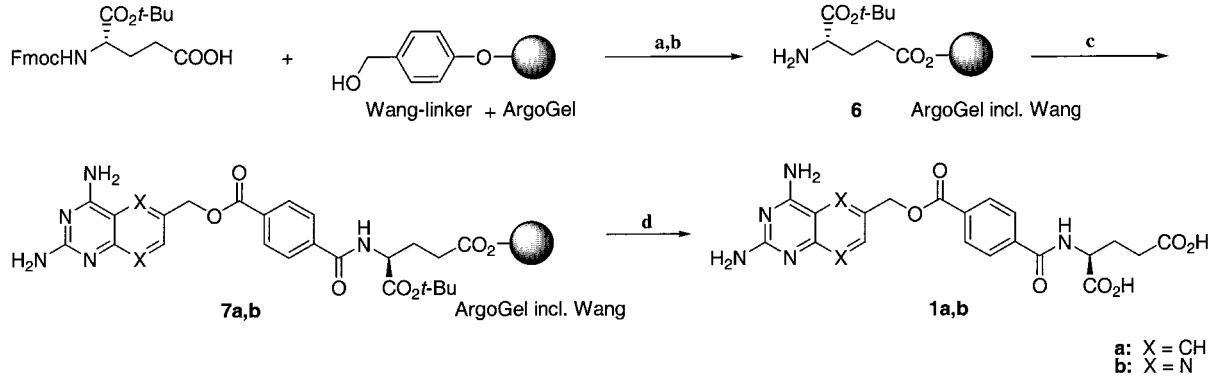


[a] Reagents and conditions: (a) DCI, 4-pyrrolidinopyridine, $CH_2Cl_2$; (b) 25% piperidine in DMF; (c) **5a** or **5b**, PyBOP, DIPEA, DMF; (d) 50% TFA/$CH_2Cl_2$.

**Table 1.** Relative Binding Free Energies

| compd A | compd B | $\Delta\Delta G_{bind}^{FEP}$(A→B) (kcal/mol)[a] | $\Delta\Delta G_{bind}^{pK_a}$(A→B) (kcal/mol)[b] | $\Delta\Delta G_{bind}$(A→B) (kcal/mol)[c] |
|---|---|---|---|---|
| MTX | **1a** | 2.9 ± 0.3 | −1.6 | 1.3 ± 0.3 |
| MTX | **1b** | 2.1 ± 0.3 | 0 | 2.1 ± 0.3 |
| **1a** | **1b** | 1.4 ± 0.6 | 1.6 | 3.0 ± 0.6 |
| **1a** | **8a** | 1.1 ± 0.5 | 0 | 1.1 ± 0.5 |
| **1b** | **8b** | 2.4 ± 1.2 | 0 | 2.4 ± 1.2 |

[a] The calculated free energy is the average of forward and backward FEP summations from independent simulations of the A → B and B → A transformations. The error given is the standard error of the mean. [b] Change in free energy of protonation of the inhibitors in solution at pH 6.9, given by eq 1. [c] Total predicted relative binding affinity = $\Delta\Delta G_{bind}^{FEP}$(A → B) + $\Delta\Delta G_{bind}^{pK_a}$(A → B).

**Table 2.** Experimental and Calculated Inhibitory Concentrations against Recombinant Human DHFR

| compd | exptl $IC_{50}$ ($\mu$M) | exptl relative $IC_{50}$ | calcd relative $K_i$[a] |
|---|---|---|---|
| MTX | 0.002[b] | 1 | 1 |
| **1a** | 0.125[b] | 63 | 9 |
| **1b** | 3.1[b] | $1.5 \times 10^3$ | 34 |
| **8a** | na[c] | na[c] | 56 |
| **8b** | na[c] | na[c] | $1.9 \times 10^3$ |

[a] Based on addition of relative free energies of binding from Table 1 along the shortest path from MTX. [b] The corresponding $IC_{50}$ values obtained with rat liver DHFR assay according to ref 46 were determined as 0.0025 $\mu$M (MTX), 0.0193 $\mu$M (**1a**), and 0.12 $\mu$M (**1b**), respectively. [c] na, not available (compound not synthesized).

to allow for comparison of the theoretical and experimental data.

**Chemical Syntheses.** Standard solution-phase chemistry was combined with solid-phase synthesis for the preparation of compounds **1a,b**. A literature method[21] starting from terephthaloyl chloride with pyridine in *tert*-butyl alcohol and subsequent monodeprotection, using potassium hydroxide in *tert*-butyl alcohol, yielded the monoester **2** (Scheme 1). A coupling reaction of 2,4-diamino-6-(bromomethyl)quinazoline (**3a**) with cesium carbonate as base in *N,N*-dimethylformamide (DMF) afforded the ester **4a** in a satisfactory yield. Selective hydrolysis of the *tert*-butoxyl group of **4a** in trifluoroacetic acid (TFA) delivered the acid **5a**.

Since previously we had experienced difficulties in the isolation of related compounds, solid-phase chemistry was introduced with the objective of simplifying purifications. Esterification of the commercially available Fmoc-Glu-OtBu was conducted on ArgoGel with the acid labile Wang linker as solid support (Scheme 2). Fmoc deprotection by 20% piperidine in DMF yielded the polymer-supported glutamic acid derivative **6**, which was further reacted with compound **5a**, using PyBOP as coupling reagent, eventually providing the amide **7a**. According to $^{13}C$ NMR the amide bond formation occurred smoothly. Hydrolysis of **7a** in 50% TFA/dichloromethane for 1.5 h cleaved both the *tert*-butyl ester and the Wang linker in one step providing the target compound **1a** in 92% yield (four steps, total yield starting from the Wang resin). The photolabile linker, P-linker-2,[22] was initially employed as an acid/base stable linker. However, since the central ester bond

**Table 3.** Plasma Pharmacokinetic Parameters[a] in Male SD Rats ($n = 3$)

a. After Intravenous Administration of MTX and Compound **1a**

| treatment | $AUC_{inf}$ (nmol/L × h) | $C_{max}$ (nmol/L) | $V_{ss}$ (L/kg) | $T_{1/2}$ (h) | CL (mL/min/kg) |
|---|---|---|---|---|---|
| MTX iv | 1559 ± 528 | 8257 ± 3684 | 0.36 ± 0.16 | 0.9 ± 0.06 | 11 ± 3.3 |
| **1a** iv | 1231 ± 489 | 9171 ± 2392 | 0.42 ± 0.076 | 1.0 ± 0.3 | 15 ± 5.4 |

b. After Oral Administration of MTX and Compound **1a**

| treatment | AUC (nmol/L × h) | $C_{max}$ (nmol/L) | $T_{max}$ (h) | $F$ (%) |
|---|---|---|---|---|
| MTX po | 838 ± 299 | 266 ± 61.6 | 0.67 ± 0.29 | 5.8 ± 2.3 |
| **1a** po | 384 ± 207 | 144 ± 30.1 | 0.67 ± 0.29 | 3.4 ± 2.0 |

[a] AUC (area under the curve), $C_{max}$ (mean peak plasma concentration), $V_{ss}$ (volume of distribution at steady state), $T_{1/2}$ (plasma half-life), CL (clearance), $T_{max}$ (time required to reach $C_{max}$), $F$ (bioavailability).

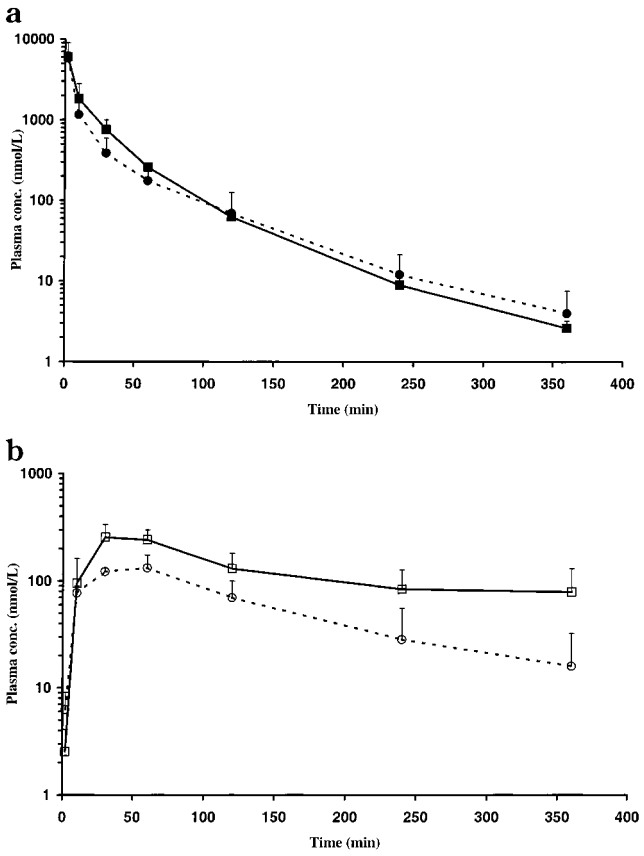


**Figure 4.** (a) Plasma concentration−time curves of MTX and compound **1a** after iv administration to male SD rats. The values are the means ± SD for three rats. The doses of MTX (■) and **1a** (●) are normalized to 1 μmol/kg. (b) Plasma concentration−time curves of MTX and compound **1a** after po administration to male SD rats. The values are the means ± SD for three rats. The doses of MTX (□) and **1a** (○) are normalized to 10 μmol/kg.

remained intact after treatment with TFA with the Wang linker, P-linker-2 offered no advantages in this case. The main disadvantage using the latter linker was that deprotection of the *tert*-butyl ester was required prior to the photolysis. Furthermore, byproducts and liberated poly(ethylene glycol) (PEG) were observed after photolysis. Neither couplings of **3a** or 2,4-diaminoquinazoline-6-methanol[15] with a polymer-supported benzoic acid derivative nor early efforts to attach the amino groups of the heterocycle to different linkers were successful. The pteridine derivative **1b** was prepared analogosly to **1a,** from commercially available 2,4-diaminopteridine-6-methanol, by the synthetic route outlined in Scheme 2.

**Dihydrofolate Reductase Assay.** Compounds **1a,b** and MTX were tested for their ability to inhibit recombinant human DHFR. The results are presented in Table 2 as $IC_{50}$ values, and also as $IC_{50}$ values relative to MTX. It was revealed that compound **1a** was approximately 60 times less potent than MTX as an inhibitor of human DHFR in the assay used. The pteridine ester **1b** exhibited a very poor inhibitory effect.

**Pharmacokinetics in Rats.** The pharmacokinetics of the quinazoline ester **1a** and of MTX were evaluated in rats after intravenous and oral administration (average plasma concentrations, corrected for differences in dose plotted versus time, are shown in Figure 4). Compound **1a** and MTX exhibited similar kinetics after intravenous administration (CL: 15 and 11 mL/min/kg, respectively). The pharmacokinetic parameters are given in Table 3. The alcohol metabolite formed after enzymatic hydrolysis and also the corresponding carboxylic acid (formed after subsequent oxidation of this alcohol) were both observed in plasma.

**Antigen-Induced Arthritis in Rats.** Two comparisons were made; first the effect of MTX administered orally was compared to that given ip. The data indicates that MTX is effective irrespective of the mode of administration although the antiarthritic effect was somewhat slower in onset in the ip group (Figure 5a). Second, the effect of compound **1a** was compared to that of MTX, where both were given ip daily. The ester analogue **1a** exerted no detectable antiarthritic effect despite that it was given in a 25 times higher dose than MTX (Figure 5b). Note that MTX is only 6 times more potent than **1a** as an inhibitor in the rat DHFR assay (Table 2, see footnotes).

## Discussion

Compound **1a** is predicted to bind to human DHFR with only 1.3 kcal/mol lower affinity than MTX; the less favorable interactions of **1a** indicated by the positive $\Delta\Delta G_{bind}^{FEP}$ are compensated in part by the difference in free energy of protonation (Table 1). From comparison of the experimental structure of the DHFR−MTX complex to the structure of **1a** at the end of the transformation of MTX shown in Figure 6, it is clear that the quinazoline ring remains tightly held in place. However, even with a well-defined binding mode of the bicyclic ring system there may be conformational alternatives regarding the positioning of the rest of the ligand. The nitrogens at positions 5 and 8 that distinguish the pteridine from the quinazoline moiety do not appear to affect the binding mode of the ring system. In fact, the only hydrogen bond from these nitrogens in

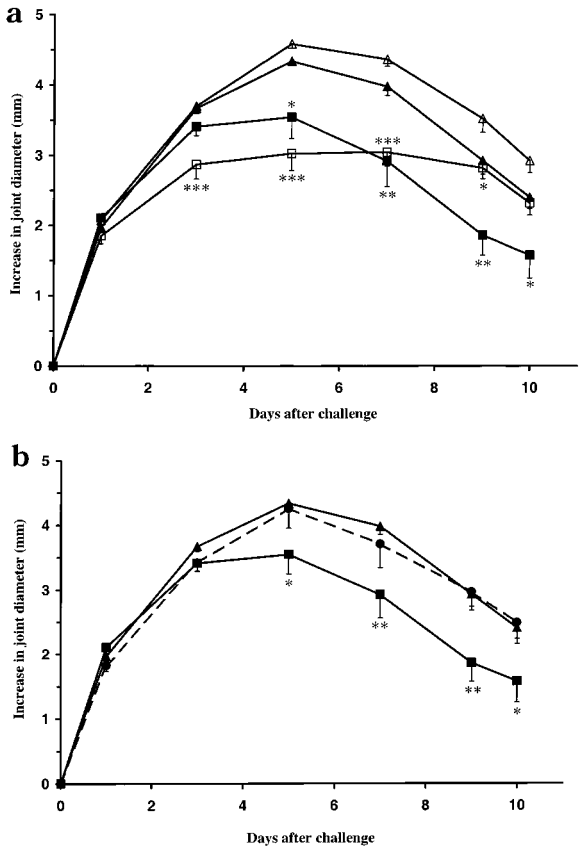


**Figure 5.** (a) Joint swelling in AIA rats ($n$ = 6/time point except vehicle po ($n$ = 5)) treated with MTX po (□, 4 mg/kg/week starting 1 week before challenge), vehicle po (saline, △), MTX ip (■, 0.15 mg/kg/day starting on the day of challenge), or vehicle ip (saline, ▲). All data are from a separate experiment and are given as mean ± SEM; *$p$ < 0.05, **$p$ < 0.01, ***$p$ < 0.001 compared to the vehicle group (Fisher's PLSD). (b) Joint swelling in AIA rats ($n$ = 6/time point) after ip doses of MTX (■, 0.15 mg/kg/day), compound **1a** (●, 3.75 mg/kg/day), or vehicle (saline, ▲) respectively. All data are from a separate experiment and are given as mean ± SEM; *$p$ < 0.05, **$p$ < 0.01 compared to the vehicle group (Fisher's PLSD).

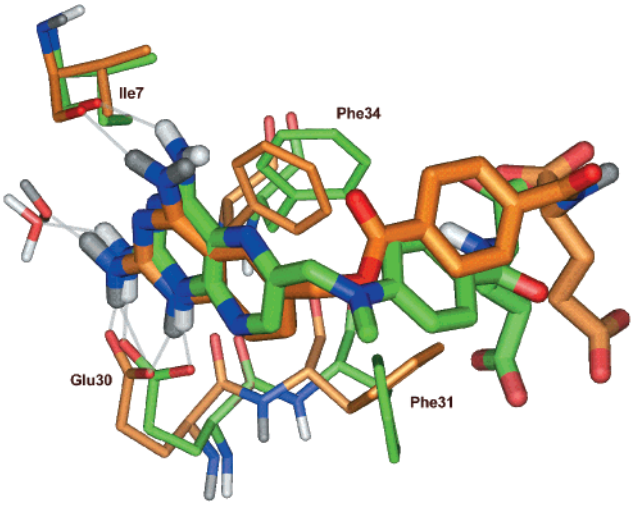


**Figure 6.** Compound **1a** in the binding site of human DHFR at the end-point of the transformation from MTX (yellow) and MTX in the crystal structure (green). Hydrogen bonds are indicated in gray. The quinazoline superimposes well on the pteridine moiety from MTX. The ester carbonyl is oriented opposite to N−$CH_3$. Interactions between the carboxylate groups and several basic side chains and water molecules are not shown.

the MTX complex structure is to a water molecule (not shown). A feature observed in nearly all the complex simulations is that the orientation of the ester carbonyl group is opposite to that of the N−$CH_3$ group in MTX as shown in Figure 6. This arrangement, while sterically different, maintains the same direction of the dipole moment of the ester linker chain as the methyleneamino linker in MTX. In the water simulations, there is a rotation about the bonds of the linker chain and no clear preference for any particular orientation of the ester group versus the bicyclic element is observed. It appears that the ester group, irrespective of the orientation of the carbonyl, is poorly 'solvated' by the protein. Transferring the more polar ester group to a rather hydrophobic pocket where it lacks specific interactions with the protein is probably unfavorable compared to the less polar N−$CH_3$ group. As expected, transformation from two- to three-atom linkers shifts the phenyl and glutamate moieties outward somewhat. We find it reassuring to see that the conformations of MTX at the end-point of the **1a** → MTX and **1b** → MTX simulations in the complex are very similar to that in the crystal structure, except for the glutamate residue which is partly exposed to the solvent. The glutamate residue of the inhibitors is very flexible, can adopt different conformations, and accepts hydrogen bonds or forms ion pairs in different ways. This can be rationalized by the presence of several positively charged side chains at similar distances around the opening to the binding site, which can make similar and interchangeable contacts with the carboxylate groups.[20]

The difference in binding free energy between the quinazoline and pteridine inhibitors is dominated by the difference in free energy of protonation, which favors the quinazolines by 1.6 kcal/mol at pH 6.9. In both the quinazoline and pteridine frameworks, extending the linker chain by one methylene group between the ester and the phenyl groups (compounds **8a**,**b**) decreases the affinity by 1.1−2.4 kcal/mol. The reason for this seems to be that the longer linker chain cannot attain a relaxed extended conformation in the complex, even though the phenyl group is pushed somewhat outward. Furthermore, the displacement of the phenyl group disturbs the interactions with Phe31 of the enzyme.

Adding relative free energies in Table 1 along the path MTX → **1a** → **1b** → MTX gives 2.2 kcal/mol. This error in closing the cycle of inhibitors is probably not due to convergence problems in the individual transformations, where results from independent forward and backward simulations agree very well. Uncertainty about the details of the binding conformation of **1a**,**b** reflected in the initial structures for the **1a** → **1b** and **1b** → **1a** simulations, which are the end-points of MTX → **1a** and MTX → **1b** simulations, respectively, may contribute to this error. A corresponding simulation starting from the docked structures of **1a** was performed for comparison and gave a $\Delta\Delta G_{bind}$ of 3.9 kcal/mol, only marginally different from the 3.0 kcal/mol reported in Table 1.

Generally, the amino acid side chains lining the binding site undergo slight conformational changes during the MD simulations, whereas backbone displacements are negligible. In a typical simulation, the root-mean-square (rms) coordinate deviations from the initial

structure for 15 active site residues was limited to about 1 Å. Hydrogen bonds and ion pairs with the pteridine/quinazoline also remain intact during all the simulations.

Long simulations and a large number of FEP steps ($\lambda$ points) were required to achieve convergence between the independent simulations of the MTX → **1a** and **1a** → MTX transformation processes. These transformations involve both the change of charge distribution between the pteridine and quinazoline ring systems and the creation and annihilation of atoms in the linker chain and are associated with large absolute values of $\Delta G_1$ and $\Delta G_2$ (ca. 100 kcal/mol). These values have no physical interpretation since they include also contribution from intramolecular interactions, whose absolute energy values are determined by the force-field logic. Most of the other transformation processes yielded nearly identical results with only one-fourth of the simulation time (4.5-ps data collection at about 60 $\lambda$ points).

The in vivo effects of MTX and **1a** were evaluated in a rat model. The amino acid sequence of the rat enzyme (*R. norvegicus*) is not available in any database. The sequence from another rodent (*M. auratus*) is 90% identical to the human DHFR enzyme. No major differences between rat and human DHFR in binding affinity of the inhibitors were expected as deduced from a homology model of the sequence of *M. auratus* showing that the residues involved in binding are conserved. This was confirmed by the experimental enzyme binding data shown in Table 2.

When MTX was given orally, the antiarthritic effect was similar to that seen after ip administration, this despite that the oral bioavailability was only about 5% (Table 3b). Part of this discrepancy could be explained by the effect of polyglutamation leading to intracellular pharmacokinetics, which most likely differ substantially from the extracellular pharmacokinetics which were measured. The total dose given was also higher in the oral group ($3 \times 4 = 12$ mg/kg) compared to the ip group ($10 \times 0.15 = 1.5$ mg/kg). It seems less likely that these factors entirely could explain the high effectiveness of the oral administration. Our reason for comparing these two groups was that we hypothesized that a large part of the effect of MTX could take place in the gut mucosa. Our results still suggest that this is possible. After oral dosing the drug concentration is likely to be higher in the gut wall than in plasma. Furthermore, one possible mechanism of action for MTX is that it could induce apoptosis in activated T-lymphocytes.[23] Since a large portion of the body's T-cells are present in the gut lymphatic system, it could simply be that a high drug concentration here is important for a strong effect.

The ester analogue **1a** had no antiarthritic effect. This result was clearly unexpected in light of the pharmacokinetic data and the effect on DHFR in vitro. A possible explanation for this discrepancy would be if the primary target for MTX in the antigen-induced arthritic model was another folate-dependent enzyme other than DHFR, e.g., AICARtf (5-aminoimidazole-4-carboxamide ribonucleotide transformylase). Despite thorough research in this area, the mechanism of action of MTX in rheumatoid arthritis is still under dispute.[23−26]

## Conclusion

It has been demonstrated that the estimation of relative binding free energies by FEP simulations can be useful for the selection of target compounds to be synthesized for biological evaluation. Both of the ester analogues, **1a**,**b**, were predicted to inhibit human DHFR, although to a lesser extent than MTX itself. Compound **1a** was predicted to be more potent than **1b**. Although a larger difference in affinity was encountered in the human DHFR assay, the calculated ranking of the ligands was correct. The analogue **1a** has a high affinity for DHFR, and despite its ester link, **1a** exhibits a similar pharmacokinetic profile to MTX. Thus, it seems that the ester link could provide a new suitable substitute for the methyleneamino bridge and other fragments connected to the ring system that are commonly found in analogues of MTX. However, in a more complex in vivo system, the antigen-induced arthritis model, the ester **1a** was not effective. A more extensive study is necessary to elucidate this particular issue.

## Experimental Section

**Computational Methods.** Relative binding affinities were calculated as relative free energies of binding using the free energy perturbation (FEP) method.[19] For another application of this method to DHFR inhibitors, see Cummins and Gready.[27] This procedure is based on a thermodynamic cycle as shown in Figure 3. From the thermodynamic cycle it follows that the relative binding affinity $\Delta\Delta G_{bind}(A \rightarrow B)$ can be calculated using:

$$\Delta\Delta G_{bind}(A \rightarrow B) = \Delta G_{bind}(B) - \Delta G_{bind}(A) = \Delta G_2 - \Delta G_1 \quad (1)$$

The free energies $\Delta G_1$ and $\Delta G_2$ pertain to the "alchemical" processes where inhibitor A is transformed into inhibitor B in solution and bound to the solvated enzyme, respectively. These processes can be simulated with moderate computational effort, as opposed to the actual binding processes. The enzyme does not affect the calculation of $\Delta G_1$, which thus only involves FEP transformation between the solvated inhibitors. The free energy associated with transforming inhibitor A into inhibitor B, whose interactions are described by the potentials $V_A$ and $V_B$, respectively, can be calculated using the perturbation formula:

$$\Delta G_i(A \rightarrow B) = -RT\sum_m \ln\langle \exp(-(V_{m'} - V_m)/RT)\rangle_m \quad (2)$$

where $i = 1$ or 2 as in eq 1. $V_m = (1 - \lambda)V_A + \lambda V_B$ are intermediate potentials used during the transformation and $\lambda \in [0,1]$ is a mapping parameter that controls the transformation between the initial and final states. The free energy is thus calculated as a sum over small steps in $\lambda$ in which $V_m$ changes to $V_{m'}$. The ensemble averages $\langle\cdot\rangle_m$ are calculated from molecular dynamics (MD) simulations on the potential $V_m$.

In a previous work[20] that addressed the calculation of absolute binding free energies the approximate linear interaction energy (LIE) method[18] was used. However, for the set of rather similar inhibitors studied here one can expect that the more rigorous FEP method should provide accurate relative binding estimates with manageable computational expense. Furthermore, the fluctuations in the inhibitors' electrostatic interaction energies with the surroundings due to the ionic groups in the glutamate moiety tend to overshadow the changes due to substitutions in the ring system and linker chain.[20] This situation makes the LIE method less suited for eliciting small changes in affinity. The difficulties to achieve convergent results with ionic groups at the ends of flexible arms remain challenging also with FEP calculations of $\Delta\Delta G$'s, although less pronounced since the relative free energies are

calculated directly rather than as the difference between two absolute values. FEP calculations on this system also poses new challenges: (1) Extending the linker chain of the inhibitors by introducing groups in the interior of the chain requires careful handling of both bonded and nonbonded interactions within the molecule to avoid excessive strain. (2) Docking of the ester-linked inhibitors is not trivial, despite the strong similarities to MTX, since an extra element in the linker chain is introduced and the dipole of the ester carbonyl group is opposite that of the $N-CH_3$ of MTX. (3) The preferred conformation of the ester group, particularly the orientation of the carbonyl, is not obvious: e.g., different orientations occurred among the highest ranked conformations generated by the docking program FLEXX.[28]

The $\Delta\Delta G$'s obtained from eq 1 can only be calculated assuming the same protonation state of the inhibitor in solution and in the complex. This is valid for the 2,4-diaminoquinazolines (p$K_a$ about 7.7)[20] but not true for the 2,4-diaminopteridines, which have a p$K_a$ of about 5.7[29] and are known to become protonated at N1 upon binding.[29] In such cases $\Delta\Delta G$ must be corrected by the free energy associated with protonation of the inhibitor in solution. This correction takes the form:

$$\Delta\Delta G_{\text{bind}}^{\text{p}K_a}(\text{A} \rightarrow \text{B}) = RT \ln 10(\text{p}K_a(\text{A}) - \text{p}K_a(\text{B})) \quad (3a)$$

when both inhibitors A and B have p$K_a$ lower than the pH at which the affinities are to be calculated. If inhibitor B has p$K_a$ > pH then the correction becomes:

$$\Delta\Delta G_{\text{bind}}^{\text{p}K_a}(\text{A} \rightarrow \text{B}) = RT \ln 10(\text{p}K_a(\text{A}) - \text{pH}) \quad (3b)$$

The free energy contribution for protonation of a 2,4-diaminopteridine to the binding free energy relative to a 2,4-diaminoquinazoline is thus calculated using eq 3b. At pH 6.9 the correction is 1.6 kcal/mol (see Table 1). The processes of transforming one inhibitor into another were carried out using hybrid molecules including all atoms particular to each of the two species, in addition to the atoms common to both. By turning appropriate atoms into 'dummy atoms' (with no interactions), in combination with altering partial charges, Lennard−Jones parameters for atoms changing type, and altering the parameters for bond angles, torsion, and improper torsion angles, the two inhibitors are modeled in the framework of the hybrid molecule. In this way the transformation between the two end-points (states) representing the two inhibitors can be carried out along a smooth pathway via intermediate linear combinations defined by a series of values for the coupling parameter $\lambda$. Very closely spaced such $\lambda$ points turned out to be necessary to achieve reasonable convergence; 116 $\lambda$ values were used to connect the initial and final states. Bonds to atoms transformed into dummy atoms were retracted to shorter lengths as required when atoms from the middle of a chain were removed. These bond lengths were constrained to the average lengths in the two end-points, weighted by $\lambda$. Interactions between atoms in 1−4 positions (connected via 2 atoms) across or with the atoms being transformed to dummy atoms were eliminated since they would otherwise lead to large artificial repulsion in the intermediate states.

The model of DHFR was taken from the crystal structure of the ternary complex of the human L22Y mutant with NADPH and MTX by Lewis et al. (PDB entry 1DLS)[30] where prior to simulations the wild-type enzyme complex was modeled from this structure. Ionic groups on the protein within about 10 Å from the inhibitor were included, whereas those far from the inhibitor were modeled as dipolar.[20] The net charge of the protein + cofactor was zero. Ligands other than MTX were docked using the FLEXX docking program.[28]

The program Q[31] was used for the MD simulations employing the GROMOS87 force field.[32] Simulations of the solvated inhibitors were carried out in 18 Å radius spheres of rigid SPC[32] water molecules with one central atom of the inhibitor restrained to the center of the sphere. The systems were equilibrated for 50 ps at 300 K. In the simulations of solvated enzyme−cofactor−inhibitor complexes, the center of the 18 Å radius sphere was fixed at the binding site and protein atoms outside this sphere (ca. 750) were not included in the simulations. Partial charges for the inhibitors were assigned as in earlier work[20] based on semiempirical AM1-SM2 calculations.[33] The complexes were equilibrated by a stepwise heating scheme during 58 ps. All simulations were carried out at 300 K with a time step of 1.5 fs. At each of the 116 $\lambda$ points the system was equilibrated for 3 ps followed by data collection during 9 ps, giving a total simulation time of 1450 ps. Independent simulations of the forward and reverse transformation processes were conducted to estimate the error of the FEP calculations.

**Chemistry. General Information.** Melting points (uncorrected) were determined in open glass capillaries on an Electrothermal apparatus. Infrared (IR) spectra were recorded on a Perkin-Elmer 1605 FT-IR spectrophotometer and are recorded in $\nu_{max}$ ($cm^{-1}$). $^1H$ and $^{13}C$ NMR spectra were recorded on a JEOL JNM-EX270 spectrometer at 270 and 67.8 MHz, respectively and a JEOL JNM-EX400 spectrometer at 400 and 100 MHz, respectively. Thin-layer chromatography (TLC) was performed by using aluminum sheets precoated with silica gel 60 $F_{254}$ (0.2 mm) type E. Merck. Chromatographic spots were visualized by UV light. Column chromatography was conducted on silica gel S (0.032−0.063 mm; Riedel-deHaën) and silica gel 60 (0.040−0.063 mm; E. Merck), unless otherwise noted. Preparative TLC was performed on glass sheets precoated with silica gel 60 $F_{254}$ (2.0 mm; E. Merck). Centrifugal chromatography was carried out on a Harrison Research Chromatotron (model 7924T) with silica gel $PF_{254}$ containing gypsum (E. Merck) as solid phase. The elemental analyses were performed by Mikro Kemi AB, Uppsala, Sweden, or Analytische Laboratorien, Gummersbach, Germany, and were within ±0.4% of the calculated values. All commercial chemicals were used without further purification. In the cases where solid-phase syntheses were adopted, washings after all reactions were performed with different combinations of solvents using DMF, methanol, and dichloromethane. All reactions on solid phase were performed in polypropylene syringe columns fitted with a polypropylene frit. The latter was also used for all the washings. $^{13}C$ NMR on solid phase were conducted in DMSO-$d_6$ to achieve adequate spectra. The loading value for the polymersupported glutamic acid derivative **6** was obtained by amino acid analysis performed at the Department of Biochemistry, Uppsala Biomedical Center, Uppsala, Sweden, on 24-h hydrolysates with a LKB 4151 alpha plus analyzer using ninhydrin detection.

**Terephthalic Acid Mono-*tert*-butyl Ester (2).**[21] Pyridine (4.0 g, 50 mmol) and *tert*-butyl alcohol (3.7 g, 49 mmol) were added to terephthaloyl chloride (5.0 g, 25 mmol). Heat was evolved and a solid cake was formed. The reaction mixture was allowed to stir overnight before it was extracted with diethyl ether and aqueous sodium bicarbonate. Drying ($MgSO_4$) and filtration yielded after concentration under reduced pressure a fine white powder, which was recrystallized from aqueous ethanol affording 4.3 g (62%) of pure diester: mp 116−117 °C (lit.[21] mp 118 °C). The diester (2.5 mg, 90 mmol) was dissolved in warm *tert*-butyl alcohol (9.3 g) and added to a mixture of potassium hydroxide (0.50 g, 9.0 mmol) in *tert*-butyl alcohol (6.8 g). The reaction mixture was warmed to 50 °C and stirred for 3 h. After cooling the solid was extracted with large volumes of chloroform and 1 M HCl (0 °C) was added and a final extraction into the organic layer was performed. Drying ($MgSO_4$) and evaporation of the organic layer under reduced pressure yielded a mixture of both starting material and product. The solid was dissolved in methanol and a small portion of silica gel was added. The silica plug was loaded on a silica column and the mixture was purified by flash chromatography [chloroform:methanol (39:1 with a gradient to 9:1)] yielding 1.35 g (85%) of **2** based on consumed starting material: $^1H$ NMR ($CDCl_3$) $\delta$ 10.50 (br s 1H, COO*H*), 8.17−8.06 (4H, Ar*H*), 1.61 (s, 9H); $^{13}C$ NMR ($CDCl_3$) $\delta$ 171.32, 164.80, 136.62, 132.54, 130.01 (2C), 129.45 (2C), 81.89, 28.12.

**2,4-Diamino-6-(bromomethyl)quinazoline (3a).** Compound **3a** was prepared according to a method described elsewhere in the preparation of **3b**[34] adding 30% hydrobromic acid in acetic acid (18 mL) to a solution consisting of 2,4-diaminoquinazoline-6-methanol[15] (0.100 g, 0.53 mmol) in acetic acid (14 mL). After stirring at room temperature for 24 h in the absence of light, the mixture was poured down to cold diethyl ether with stirring and allowed to stand in the refrigerator for a couple of hours before the precipitate was collected under nitrogen and washed with cold diethyl ether. The formed hydrobromic salt was dried in vacuo at 40 °C before it was used in the next step without further purification.

***tert*-Butyl 4-[(2,4-Diaminoquinazolin-6-yl)methoxycarbonyl]benzoate (4a).** Freshly prepared **3a** (0.53 mmol) was added portionwise to a mixture of compound **2** (0.351 g, 1.58 mmol) and cesium carbonate (0.514 g, 1.58 mmol) in anhydrous DMF (15 mL). The reaction mixture was allowed to stir at room temperature for 5 days before it was filtered. A small portion of silica gel was added and the solvent was evaporated under reduced pressure. The silica plug was added on the top of a silica column and the product was purified by flash chromatography [chloroform:methanol (39:1) + aqueous $NH_3$] providing 65 mg (31% over 2 steps) after a further purification by circular chromatography [chloroform:methanol (39:1) + aqueous $NH_3$]: IR (KBr) 1715 (ester) $cm^{-1}$; $^1H$ NMR (DMF-$d_6$) $\delta$ 8.24 (d, $J$ = 1.81 Hz, 1H, *H*-5), 8.18−8.08 (m, 4H, Ar*H*), 7.68 (dd, $J$ = 8.58, 1.81 Hz, 1H, *H*-7), 7.44 (br s, 2H, N$H_2$), 7.29 (d, $J$ = 8.58 Hz, 1H, *H*-8), 6.10 (br s, 2H, N$H_2$), 5.42 (s, 2H), 1.59 (s, 9H); $^{13}C$ NMR (DMF-$d_6$) $\delta$ 171.84, 165.61, 164.77, 163.43, 135.58, 136.11, 134.05, 133.22, 129.88 (2C), 129.73 (3C), 127.83, 125.43, 124.26, 110.64, 67.48, 27.71 (3C). Anal. ($C_{21}H_{22}N_4O_4$) C, H, N.

**4-[(2,4-Diaminoquinazolin-6-yl)methoxycarbonyl]benzoic Acid (5a).** Compound **4a** (39 mg, 0.10 mmol) in trifluoroacetic acid (1 mL) was allowed to stir at room temperature for 2 h before the solvent was evaporated under reduced pressure. The crude product was triturated with diethyl ether and the formed precipitate was filtered off. Water was added and the pH was adjusted to 3.8. The flask was stored in the refrigerator overnight, filtered and washed with water, acetone, and diethyl ether, respectively, providing 22 mg (67%) of a white solid: IR (KBr) 1713 (ester) $cm^{-1}$; $^1H$ NMR (DMSO-$d_6$ + 1 drop of $DCO_2D$) $\delta$ 8.32 (app s, 1H, *H*-5), 8.11−8.05 (m, 4H, Ar*H*), 7.90−7.88 (m, 1H), 7.48−7.45 (m, 1H), 5.41 (s, 2H); $^{13}C$ NMR (DMSO-$d_6$ + 1 drop of $DCO_2D$) $\delta$ 166.94, 165.50, 163.24, 154.88, 139.29, 135.75, 135.25, 133.33, 132.46, 129.91 (4C), 124.81, 117.53, 109.53, 66.32. Anal. ($C_{17}H_{14}N_4O_4 \cdot 0.5CF_3CO_2H \cdot 1H_2O$) C, H, N.

**Polymer-Supported Glutamic Acid Derivative 6.** Argo-Gel-Wang-OH (0.5 g, 0.21 mmol) was allowed to swell in dichloromethane (8 mL). Fmoc-Glu-OtBu (0.45 g, 1.05 mmol), *N*,*N*′-diisopropylcarbodiimide (163 $\mu$L, 1.05 mmol) and 4-pyrrolidinopyridine (15 mg, 0.10 mmol) were added and the vessel was capped and placed in an overhead mixer for 4 h. The reaction liquors were removed by filtering and the resin was washed with dichloromethane, methanol, DMF and dichloromethane, respectively. A mixture of 25% piperidine in DMF was added to cleave off the Fmoc protecting group and after 15 min the solid phase was washed again with DMF, methanol, and dichloromethane, respectively and dried in vacuo overnight: $^{13}C$ NMR (DMSO-$d_6$) $\delta$ 174.83, 173.09, 158.81 (Wang), 129.97 (2C, Wang), 128.25 (Wang), 114.57 (2C, Wang), 81.11 ($C(CH_3)_3$), 70.56 (PEG), 67.43 (PEG), 66.04 (Wang), 54.26 (CH), 30.73, 29.85, 28.04 (C($CH_3$)$_3$). Amino acid analysis: Glu, 0.42 mmol/g.

**Polymer-Supported 2,4-Diaminoquinazoline Derivative 7a.** The resin **6** (0.200 g, 84 $\mu$mol) was swelled for about 10 min in DMF (7 mL). PyBOP (131 mg, 0.25 mmol), *N*,*N*-diisopropylethylamine (88 $\mu$L, 0.50 mmol) and compound **5a** (85 mg, 0.25 mmol) were added. The reaction proceeded for 4 h before the suspension was filtered off. The resin was washed with DMF, methanol, and dichloromethane, respectively: $^{13}C$ NMR (DMSO-$d_6$) $\delta$ 172.07, 170.67, 165.84, 165.13, 162.49, 160.94 (Wang), 158.34, 152.31, 138.01, 133.00, 131.99, 129.82 (2C, Wang), 129.21 (2C), 127.82 (2C), 127.04 (Wang), 124.31 (2C), 114.25 (2C, Wang), 109.92, 80.68 ($C(CH_3)_3$), 69.76 (PEG), 68.23 (PEG), 67.09 (PEG), 66.86, 65.34 (Wang), 52.68 (CH), 30.21, 27.56 (C($CH_3$)$_3$), 25.71.

***N*-[4-[(2,4-Diaminoquinazolin-6-yl)methoxycarbonyl]-benzoyl]-L-glutamic Acid (1a).** The resin **7a** (0.200 g, 0.42 mmol) was treated with 50% TFA/dichloromethane (6 mL) for 1.5 h. The product was filtered off and washed with dichloromethane, DMF, methanol, and dichloromethane, respectively. The first washing fraction from the washing with dichloromethane was evaporated under reduced pressure. The following workup procedure was the same as for compound **5a**, yielding 36 mg of the final compound (92% over 4 steps): IR (KBr) 1724 (ester), 1652 (amide) $cm^{-1}$; $^1H$ NMR (DMSO-$d_6$) $\delta$ 8.73 (d, $J$ = 7.75 Hz, 1H, N*H*), 8.20 (app d, 1H, *H*-5), 8.10−7.98 (m, 4 + 2H, Ar*H* + N$H_2$), 7.83 (br s, 2H, N$H_2$), 7.74 (dd, $J$ = 8.58, 1.65 Hz, 1H, *H*-7), 7.32 (d, $J$ = 8.58 Hz, 1H, *H*-8), 7.09 (br s, 2H, N$H_2$), 5.37 (s, 2H), 4.42−4.34 (m, 1H), 2.35 (app t, 2H), 2.16−1.88 (m, 4H); $^{13}C$ NMR (DMSO-$d_6$) $\delta$ 174.06, 173.84, 165.51, 165.12, 162.65, 158.54, 138.42, 133.98, 131.77, 129.28 (2C), 128.93, 127.80 (2C), 124.29, 121.27, 109.46, 66.52, 52.44, 30.72, 26.31 (one aromatic carbon missing). Anal. ($C_{22}H_{21}N_5O_7 \cdot 1H_2O$) C, H, N.

**4-[(2,4-Diaminopteridin-6-yl)methoxycarbonyl]benzoic Acid (5b).** Compound **5b** was prepared as described above in the synthesis of **5a** starting from 1.56 mmol of 2,4-diamino-6-(bromomethyl)pteridine (**3b**)[35] and compound **2** (643 mg, 2.89 mmol) in the presence of cesium carbonate (2.5 g, 7.67 mmol). The reaction mixture was allowed to stir at room temperature in dry DMF (15 mL) for 2 days. After filtration and purification 132 mg of **4b** together with the byproduct in the reaction (2,4-diaminopteridine 6-methylacetate) was collected and allowed to react further with trifluoroacetic acid (7 mL). Workup and purification was performed following the same procedure as for **5a** yielding 77 mg of **5b** as the only product (10% over 2 steps): $^1H$ NMR (DMSO-$d_6$) $\delta$ 8.90 (s, 1H, *H*-7), 8.13−8.04 (m, 4H, Ar*H*), 7.84 (br s, 2H, N$H_2$), 6.86 (br s, 2H, N$H_2$), 5.49 (s, 2H); $^{13}C$ NMR (DMSO-$d_6$) $\delta$ 167.13, 165.54, 163.37, 163.11, 155.52, 150.88, 143.44, 135.60, 133.39, 130.21 (4C), 122.25, 66.24. Anal. ($C_{15}H_{12}N_6O_4 \cdot 0.25CF_3CO_2H \cdot 0.5H_2O$) C, H, N.

**Polymer-Supported 2,4-Diaminopteridine Derivative 7b.** Compound **7b** was prepared as described for **7a** starting from **6** (150 mg, 63 $\mu$mol) and **5b** (77 mg, 2.26 mmol): $^{13}C$ NMR (DMSO-$d_6$) $\delta$ 172.42, 170.88, 166.17, 165.16, 163.40, 163.11, 158.44 (Wang), 155.86, 150.61, 142.60, 138.25, 134.91, 131.71 (Wang), 129.95 (Wang + 2C), 129.52 (Wang + 2C), 122.11, 114.35 (Wang), 81.11 ($C(CH_3)_3$), 69.90, 67.20, 65.73, 62.71, 52.90, 30.41, 27.68 (C($CH_3$)$_3$), 25.88.

***N*-[4-[(2,4-Diaminopteridin-6-yl)methoxycarbonyl]benzoyl]-L-glutamic Acid (1b).** The resin **7b** was treated with 50% TFA/dichloromethane as in the case for **7a**, yielding 14 mg of the final compound: $^1H$ NMR (DMSO-$d_6$) $\delta$ 8.90 (s, 1H, *H*-8), 8.79 (d, $J$ = 7.92 Hz, 1H, N*H*), 8.12−7.98 (m, 4H, Ar*H*), 7.68 (br s, 2H, N$H_2$), 6.74 (br s, 2H, N$H_2$), 5.48 (s, 2H), 4.45−4.36 (m, 1H), 2.38−2.33 (m, 2H), 2.12−1.91 (m, 2H); $^{13}C$ NMR (DMSO-$d_6$) $\delta$ 173.82, 173.16, 165.59, 165.05, 163.24, 162.80, 155.74, 150.33, 142.35, 138.22, 131.58, 129.35 (2C), 127.85 (2C), 121.60, 65.64, 52.11, 30.53, 25.98. Anal. ($C_{20}H_{19}N_7O_7 \cdot 0.25CF_3CO_2H \cdot 0.75H_2O$) C, H; N: calcd, 19.2; found, 18.5.

**Dihydrofolate Reductase Assay.** A plasmid with a cloned gene encoding hDHFR was a generous gift from Raymond Blakley (St. Jude Children's Research Hospital). Plasmid DNA was introduced into the *E. coli* strain DH5$\alpha$[36] by transformation. A 400-mL culture of transformed bacteria was grown in LB medium[37] to 2 × $10^8$ cells, and expression of hDHFR was induced by addition of isopropyl $\beta$-D-thiogalactopyranoside to 1 mM. Four hours after induction the cells were harvested by centrifugation, washed with 100 mL of buffer A (0.05 M Tris-hydrochloride (pH 7.2), 0.05 M potassium chloride, 1 mM dithiothreitol, 1 mM disodium EDTA), recentrifuged and finally resuspended in 3 mL of buffer A. The cells were disrupted by sonication and the DHFR was purified further as described by Tennhammar-Ekman and Sköld.[38] Reduced nicotinamide adenine dinucleotide phosphate (NADPH) was

obtained from Sigma. Dihydrofolic acid was prepared according to Blakley[39] and concentrations was determined by UV absorption using $\Delta\epsilon_{285}$ of 20 400 $M^{-1}$ $cm^{-1}$. The buffer used throughout the studies consisted of 0.02 M phosphate (potassium), pH 6.9, 1 mM dithiothreitol, 1 mM ethylenediaminetetraacetic acid (EDTA). Final concentrations (in 2 mL of buffer) were 60 $\mu$M NADPH, 36 $\mu$M dihydrofolate, and different concentrations of the inhibitor. DHFR activity was observed by following the decline in absorbance at 340 nm (NADPH maximum) using a spectrophotometric assay monitoring the decrease in absorbance of the assay mixture at 30 °C with a Beckman DU 62 spectrophotometer. The cuvettes had a light path of 1 cm. Each compound was prepared as a stock solution in buffer A. In a few cases DMSO was needed, but the final concentrations of DMSO in the enzymatic assay were in these cases less than 1%. Assays were performed, by incubating the enzyme, NADPH, and the inhibitor in the buffer for 3 min before dihydrofolate was added. The initial reaction rates were determined and monitored continuously for 5 min. The activity of recombinant human DHFR was assayed without inhibitor, together with a series of concentrations suitable for $IC_{50}$ determinations. The specific activity of the enzyme was 7.8 units/mg of protein, where 1 unit is defined as $\Delta$340 nm/min. Triplicate determinations were done at each concentration, and the results were averaged. The concentrations of inhibitor required to reduce DHFR activity by 50% ($IC_{50}$) were determined by semilogarithmic plots of the data yielding normal sigmoidal curves for most inhibitors using GraphPad Prism (version 2.01 for Windows; GraphPad Software Inc., San Diego, CA).

**Pharmacokinetics in Rats.** The pharmacokinetics of MTX and **1a** were evaluated in male SD rats, weighing 233−264 g, after intravenous (1 $\mu$mol/kg) and oral (10 $\mu$mol/kg) administration, three animals for each route of administration. The test compounds were dissolved in a DMA:PEG400:citrate buffer (40:40:20) vehicle to the concentration of 2 $\mu$mol/mL. The intravenous dose (100 $\mu$L) was given as a bolus into a tail vein. The oral dose (1 mL) was given by gavage. Blood was collected by repeated sampling from the tail vein opposite to the intravenous administration site at 2, 10, 30, 60, 120, 240, and 360 min. No anaesthetics were used during the experiment. Plasma, prepared by centrifugation of the blood for 5 min at 3000*g* in 4 °C, was precipitated with ethanol and the supernatant was analyzed for content of compound using LC−MS/MS technique. In the case of compound **1a**, the metabolites were also quantified. As standards for the bioanalysis, the test formulations were added to blank plasma and diluted stepwise giving rise to standard curves ranging from 2000 to 6000 nM. The concentration of compound in the test formulations was determined before and after each experiment by LC−MS. For calculation of the pharmacokinetic parameters, the noncompartmental analysis model in WinNonlin Professional (version 2.1; Scientific Consulting) was used.

**Antigen-Induced Arthritis (AIA): Induction and Evaluation.** MTX is presently the drug of choice for the treatment of rheumatoid arthritis (RA). MTX is one of the few antirheumatoid drugs that works both in animal models and patients. The models thus offer suitable in vivo systems for evaluation of MTX and related analogues. One such model is the AIA in rats. The acute joint inflammation in this model resembles in several respects the corresponding reaction in RA patients.[40−43] AIA is ameliorated by MTX when administrated in a similar way as in the clinic (weekly oral dosing). The exact mechanism of action is not established, but since folate supplementation in excess can override the antiarthritic effect of MTX, it is concluded that folate antagonism is essential.[26] The effect of weekly dosing which propably indicates that it is trapped intracellularly due to polyglutamation.[44]

The AIA model is also sensitive to oral tolerance: that is, inhibition of arthritis by oral feeding of the arthritogenic antigen prior to immunization, indicating a possible connection between lymphoid organs in the gut and the antigen-presenting cells in the joint. Oral tolerance has been shown to be abrogated by MTX[45] which suggests that this connection is folate-dependent, possibly at the mucosal level. In the present experiments we attempted to compare ip administration of compound **1a** and MTX to oral administration, which could give hints to the site of action. We chose an oral dosing that previously had been proven to be effective (4 mg/kg/week, starting 1 week before challenge). The ip dose was chosen based on results in preliminary experiments (0.15 mg/kg/day, starting on the day of challenge). Since we did not know the rate of polyglutamation for compound **1a** and the bioavailability seemed to be lower than that for MTX (see Table 3), we administered **1a** daily, given by ip injections. Compound **1a** was given in a high dose (3.75 mg/kg/day) in order to maximize the chance to detect an antiarthritic effect.

AIA was induced in female Dark Agouti rats with an approximate body weight of 165 g. The rats were obtained from Möllegaards Breeding Center (Denmark) and kept in sawdust-covered cages with food and water ad libitum. The temperature was thermostatically maintained at 22 °C, the relative humidity was 50%, and the light was on in 12-h periods from 6 a.m. to 6 p.m. The rats were conditioned at least one week before immunization. The experiments were approved by the Animal Ethics Committee of Lund, Sweden. The animals were killed after the last day of measurement.

For induction of AIA the rats were sensitized intradermally at the tail root with 1 mg of methylated bovine serum albumin (mBSA) dissolved in 50 $\mu$L of saline and emulsified in 50 $\mu$L of Freund's complete adjuvant. Ten days later the rats were challenged with a unilateral intraarticular injection of 50 $\mu$g of mBSA (1 $\mu$g/$\mu$L, dissolved in saline). The intensity of the arthritis was quantified by measurement of joint swelling. This measure mainly reflects the pannus mass.[41] The same measure is also important for the assessment of clinical RA development. In the AIA model this parameter has a low variance and it is the only nonradiological method to follow the joint process longitudinally in single animals. For each day of measurement the increase in joint diameter for each animal was calculated. The individual values were then used in the statistical analysis. Unless stated otherwise, the area under the curve (AUC) was calculated for each animal and these values were used in the statistical analysis, which was performed by analysis of variance followed by the Fisher protected least-significant difference (PLSD). Calculations were performed on an Apple computer using StatView 4.0 (Berkeley, CA) as software. In all experiments each group contained six animals and each experiment contained a vehicle-treated control group. All presented data in Figure 5 are from a separate experiment and are given as mean ± SEM.

**Acknowledgment.** We thank Prof. Sherry F. Queener for skillful in vitro binding experiments on rat liver DHFR. We also thank the Swedish Research Council for Engineering Sciences (TFR), the Swedish Natural Science Research Council (NFR), and the Swedish Foundation for Strategic Research (SSF) for financial support.

## References

(1) Andersen, P. A.; West, S. G.; O'Dell, J. R.; Via, C. S.; Claypool, R. G.; Kotzin, B. L. Weekly Pulse Methotrexate in Rheumatoid Arthritis. Clinical and Immunologic Effects in a Randomized, Double-Blind Study. *Ann. Intern. Med.* **1985**, *103*, 489−496.

(2) Williams, H. J.; Willkens, R. F.; Samuelson, C. O. J.; Alarcón, G. S.; Guttadauria, M.; Yarboro, C.; Polisson, R. P.; Weiner, S. R.; Luggen, M. E.; Billingsley, L. M.; Dahl, S. L.; Egger, M. J.; Reading, J. C.; Ward, J. R. Comparison of Low-Dose Oral Pulse Methotrexate and Placebo in the Treatment of Rheumatoid Arthritis. A Controlled Clinical Trial. *Arthritis Rheum.* **1985**, *28*, 721−730.

(3) Weinblatt, M. E.; Coblyn, J. S.; Fox, D. A.; Fraser, P. A.; Holdsworth, D. E.; Glass, D. N.; Trentham, D. E. Efficacy of Low-Dose Methotrexate in Rheumatoid Arthritis. *N. Engl. J. Med.* **1985**, *312*, 818−822.

(4) Van Scott, E. J.; Auerbach, R.; Weinstein, G. D. Parenteral Methotrexate in Psoriasis. *Arch. Dermatol.* **1964**, *89*, 550−556.

(5) Rees, R. B.; Bennett, J. H.; Maibach, H. I.; Arnold, H. L. Methotrexate for Psoriasis. *Arch. Dermatol.* **1967**, *95*, 2−11.

(6) Weinstein, G. D.; Frost, P. Methotrexate for Psoriasis. A New Therapeutic Schedule. *Arch. Dermatol.* **1971**, *103*, 33−38.
(7) Mullarkey, M. F.; Blumenstein, B. A.; Andrade, W. P.; Bailey, G. A.; Olason, I.; Wetzel, C. E. Methotrexate in the Treatment of Corticosteroid-Dependent Asthma. A Double-Blind Crossover Study. *N. Engl. J. Med.* **1988**, *318*, 603−607.
(8) Mullarkey, M. F.; Webb, D. R.; Pardee, N. E. Methotrexate in the Treatment of Steroid-Dependent Asthma. *Ann. Allergy* **1986**, *56*, 347−350.
(9) Kozarek, R. A.; Patterson, D. J.; Gelfand, M. D.; Botoman, V. A.; Ball, T. J.; Wilske, K. R. Methotrexate Induces Clinical and Histologic Remission in Patients with Refractory Inflammatory Bowel Disease. *Ann. Intern. Med.* **1989**, *110*, 353−356.
(10) Peppercorn, M. A. Advances in Drug Therapy for Inflammatory Bowel Disease. *Ann. Intern. Med.* **1990**, *112*, 50−60.
(11) DeGraw, J. I.; Colwell, W. T.; Piper, J. R.; Sirotnak, F. M.; Smith, R. L. New Analogs of Methotrexate in Cancer and Arthritis. *Curr. Med. Chem.* **1995**, *2*, 630−653.
(12) Klepser, M. E.; Klepser, T. B. Drug Treatment of HIV−Related Opportunistic Infections. *Drugs* **1997**, *53*, 40−73.
(13) Queener, S. F.; Bartlett, M. S.; Jay, M. A.; Durkin, M. M.; Smith, J. W. Activity of Lipid-Soluble Inhibitors of Dihydrofolate Reductase Against *Pneumocystis carinii* in Culture and in a Rat Model of Infection. *Antimicrob. Agents Chemother.* **1987**, *31*, 1323−1327.
(14) Kovacs, J. A.; Allegra, C. J.; Swan, J. C.; Drake, J. C.; Parrillo, J. E.; Chabner, B. A.; Masur, H. Potent Antipneumocystis and Antitoxoplasma Activites of Piritrexim, a Lipid Soluble Antifolate. *Antimicrob. Agents Chemother.* **1988**, *32*, 430−433.
(15) Graffner-Nordberg, M.; Sjödin, K.; Tunek, A.; Hallberg, A. Synthesis and Enzymatic Hydrolysis of Esters, Constituting Simple Models of Soft Drugs. *Chem. Pharm. Bull. (Tokyo)* **1998**, *46*, 591−601.
(16) Lamb, M. L.; Jorgensen, W. L. Computational Approaches to Molecular Recognition. *Curr. Opin. Chem. Biol.* **1997**, *1*, 449−457.
(17) Oprea, T. I.; Marshall, G. R. Receptor-Based Prediction of Binding Affinities. *Perspect. Drug Discovery Des.* **1998**, *9*, 35−61.
(18) Hansson, T.; Marelius, J.; Åqvist, J. Ligand Binding Affinity Prediction by Linear Interaction Energy Methods. *J. Comput.-Aided Mol. Des.* **1998**, *12*, 27−35.
(19) Kollman, P. Free Energy Calculations: Applications to Chemical and Biochemical Phenomena. *Chem. Rev.* **1993**, *93*, 2395−2417.
(20) Marelius, J.; Graffner-Nordberg, M.; Hansson, T.; Hallberg, A.; Åqvist, J. Computation of Affinity and Selectivity: Binding of 2,4-Diaminopteridine and 2,4-Diaminoquinazoline Inhibitors to Dihydrofolate Reductases. *J. Comput.-Aided Mol. Des.* **1998**, *12*, 119−131.
(21) Buckle, D. R.; Smith, H. An Improved Synthesis of Substituted Benzoyl Acetates. *J. Chem. Soc.* **1971**, 2821−2823.
(22) Åkerblom, E. B.; Nygren, A. S.; Agback, K. H. Six New Photolabile Linkers for Solid-Phase Synthesis. 1. Methods of Preparation. *Mol. Divers.* **1998**, *3*, 137−148.
(23) Genestier, L.; Paillot, R.; Fournel, S.; Ferraro, C.; Miossec, P.; Revillard, J.-P. Immunosuppressive Properties of Methotrexate: Apoptosis and Clonal Deletion of Activated Peripheral T cells. *J. Clin. Invest.* **1998**, *102*, 322−328.
(24) Bannwarth, B.; Labat, L.; Moride, Y.; Schaeverbeke, T. Methotrexate in Rheumatoid Arthritis. An Update. *Drugs* **1994**, *47*, 25−50.
(25) Cronstein, B. N. Molecular Therapeutics. Methotrexate and its Mechanism of Action. *Arthritis Rheum.* **1996**, *39*, 1951−1960.
(26) Andersson, S. E.; Johansson, L.-H.; Lexmüller, K.; Ekström, G. M. Anti-Arthritic Effect of Methotrexate: Is It Really Mediated by Adenosine? *Eur. J. Pharm. Sci.* **2000**, *9*, 333−343.
(27) Cummins, P. L.; Gready, J. E. Computer-Aided Drug Design: A Free Energy Perturbation Study on the Binding of Methyl-substituted Pterins and N5-Deazapterins to Dihydrofolate Reductase. *J. Comput-Aided Mol. Des.* **1993**, *7*, 535−555.
(28) Rarey, M.; Kramer, B.; Lengauer, T.; Klebe, G. A Fast Flexible Docking Method using an Incremental Construction Algorithm. *J. Mol. Biol.* **1996**, *261*, 470−489.
(29) Cocco, L.; Roth, B.; Temple, C. J.; Montgomery, J. A.; London, R. E.; Blakley, R. L. Protonated State of Methotrexate, Trimethoprim, and Pyrimethamine Bound to Dihydrofolate Reductase. *Arch. Biochem. Biophys.* **1983**, *226*, 567−577.
(30) Lewis, W. S.; Cody, V.; Galitsky, N.; Luft, J. R.; Pangborn, W.; Chunduru, S. K.; Spencer, H. T.; Appleman, J. R.; Blakley, R. L. Methotrexate-resistant Variants of Human Dihydrofolate Reductase with Substitutions of Leucine 22: Kinetics, Crystallography, and Potential as Selectable Markers. *J. Biol. Chem.* **1995**, *270*, 5057−5064.
(31) Marelius, J.; Kolmodin, K.; Feierberg, I.; Åqvist, J. Q: An Molecular Dynamics Program for Free Energy Calculations and Empirical Valence Bond Simulations in Biomolecular Systems. *J. Mol. Graph. Model.* **1998**, *16*, 213−225.
(32) van Gunsteren, W. F.; Berendsen, H. J. C. *Groningen Molecular Simulation (GROMOS) Library Manual;* Biomos B.V.: Groningen, 1987.
(33) Cramer, C. J.; Truhlar, D. G. An SCF Solvation Model for the Hydrophobic Effect and Absolute Free Energies of Aqueous Solvation. *Science* **1992**, *256*, 213−217.
(34) Piper, J. R.; Johnson, C. A.; Maddry, J. A.; Malik, N. D.; McGuire, J. J.; Otter, G. M.; Sirotnak, F. M. Studies on Analogues of Classical Antifolates Bearing the Naphthoyl Group in Place of Benzoyl in the Side Chain. *J. Med. Chem.* **1993**, *36*, 4161−4171.
(35) Piper, J. R.; Montgomery, J. A. Preparation of 6-(Bromomethyl)-2,4-pteridinediamine Hydrochloride and Its Use in Improved Synthesis of Methotrexate and Related Compounds. *J. Org. Chem.* **1977**, *42*, 208−211.
(36) Hanahan, D. Studies on Transformation of *Escherichia coli* with Plasmids. *J. Mol. Biol.* **1983**, *166*, 557−580.
(37) Bertani, G. Studies on Lysogenesis. I. The Mode of Phage Liberation by Lysogenic *Escherichia coli*. *J. Bacteriol.* **1951**, *62*, 293−300.
(38) Tennhammar-Ekman, B.; Sköld, O. Trimethoprim Resistance Plasmids of Different Origin Encode Different Drug-Resistant Dihydrofolate Reductases. *Plasmid* **1979**, *2*, 334−346.
(39) Blakley, R. L. Crystalline Dihydropteroylglutamic Acid. *Nature* **1960**, *188*, 231−232.
(40) Andersson, S. E.; Lexmüller, K.; Ekström, G. M. Physiological Characterisation of mBSA Antigen-Induced Arthritis in the Rat. I. Vascular Leakiness and Pannus Growth. *J. Rheumatol.* **1998**, *25*, 1772−1777.
(41) Andersson, S. E.; Johansson, A.; Lexmüller, K.; Ekström, G. M. Physiological Characterization of mBSA Antigen Induced Arthritis in the Rat. II. Joint Blood Flow, Glucose Metabolism, and Cell Proliferation. *J. Rheumatol.* **1998**, *25*, 1778−1784.
(42) Andersson, S. E.; Lexmüller, K.; Johansson, A.; Ekström, G. M. Tissue and Intracellular pH in Normal Periarticular Soft Tissue and During Different Phases of Antigen-Induced Arthritis in the Rat. *J. Rheumatol.* **1999**, *26*, 2018−2024.
(43) Andersson, S. E.; Lexmüller, K.; Alving, K.; Ekström, G. M. Periarticular Tissue Levels of Cytokine- and Endothelin-1-like Immunoreactivity During the Course of Antigen-induced Arthritis in the Rat. *Inflamm. Res.* **1999**, *48*, 491−496.
(44) Cichowicz, D. J.; Shane, B. Mammalian Folylpoly-$\gamma$-glutamate Synthetase. 1. Purification and General Properties of the Hog Liver Enzyme. *Biochemistry* **1987**, *26*, 504−512.
(45) Ekström, G. M.; Szajewski, K.; Persson, Å. Commonly Used RA Drugs Abrogate Oral Tolerance in Antigen-Induces Arthritis (AIA). *Scand. J. Immunol.* **1997**, *45*, 566.
(46) Broughton, M. C.; Queener, S. F. *Pneumocystis carinii* Dihydrofolate Reductase Used to Scren Potential Antipneumocystis Drugs. *Antimicrob. Agents Chemother.* **1991**, *35*, 1348−1355.

JM0009639